

# A level-set method for thermal motion of bubbles and droplets

Néstor Balcázar<sup>1</sup>, Assensi Oliva<sup>1</sup>, Joaquim Rigola<sup>1</sup>

<sup>1</sup> Heat and Mass Transfer Technological Centre (CTTC), Universitat Politècnica de Catalunya - BarcelonaTech (UPC), ESEIAAT, Carrer Colom 11, 08222 Terrassa (Barcelona), Spain.

E-mail: [nestor@cttc.upc.edu](mailto:nestor@cttc.upc.edu)

**Abstract.** A conservative level-set model for direct simulation of two-phase flows with thermocapillary effects at dynamically deformable interface is presented. The Navier-Stokes equations coupled with the energy conservation equation are solved by means of a finite-volume/level-set method. Some numerical examples including thermocapillary motion of single and multiple fluid particles are computed by means of the present method. The results are compared with analytical solutions and numerical results from the literature as validations of the proposed model.

## 1. Introduction

When a fluid particle (bubble or drop) is placed in a second fluid in which a temperature gradient is imposed, it will move from the region with higher temperature to that with lower temperature so that the surface energy is minimized. This effect is called thermocapillary or Marangoni migration. It arises as a consequence of the local surface tension gradients on the fluid-fluid interface caused by temperature distribution. In addition to its importance from a fundamental point of view, it provides a particularly attractive means for manipulation of continuous fluid streams or fluid particles, in applications involving microgravity [1] or microdevices [2].

The thermocapillary motion of a drop was first examined experimentally by [3], who also found an analytical expression for its terminal velocity in the creeping flow limit (YGB theory), in which convective transport of momentum and heat can be neglecting. Since then, many works have been performed experimentally, analytically and numerically [4, 5]; most of the research on this phenomenon has been summarized by [1]. Additionally some numerical methods have been developed to include the deformation of the droplets, however, to the best of the author's knowledge there are not previous works on thermocapillary motion by means of the conservative level-set method [6, 7, 8]. Therefore, it is the purpose of this work to introduce a general numerical technique for simulating thermocapillary motion of deformable fluid particles, so that effects such as heat convection, container walls or the interaction of multiple fluid particles can be included. Thus, this paper contains the modeling and implementation of the thermal Marangoni stresses within the framework of the unstructured finite-volume/level-set solver introduced in our previous papers [6, 7]. This paper is organized as follows: The governing equations and numerical method are presented in section 2. Numerical results are included in section 3. Concluding remarks and future work are discussed in section 4.



## 2. Governing equations and numerical method

The Navier-Stokes equations for the dispersed fluid in  $\Omega_d = \Omega_d^1 \cup \dots \cup \Omega_d^{n_d}$  and continuous fluid in  $\Omega_c$  can be combined into a set of equations in a global domain  $\Omega = \Omega_d \cup \Omega_c$ , with a singular source term for the surface tension force at the interface  $\Gamma = \Gamma_1 \cup \dots \cup \Gamma_{n_d}$ :

$$\frac{\partial(\rho \mathbf{v})}{\partial t} + \nabla \cdot (\rho \mathbf{v} \mathbf{v}) = -\nabla p + \nabla \cdot \mu (\nabla \mathbf{v} + (\nabla \mathbf{v})^T) + \rho \mathbf{g} + \mathbf{f}_\sigma(T)$$

$$\nabla \cdot \mathbf{v} = 0 \quad (1)$$

$$\rho = \rho_d H_d + \rho_c (1 - H_d) \quad \mu = \mu_d H_d + \mu_c (1 - H_d) \quad (2)$$

where  $\mathbf{v}$  and  $p$  denote the fluid velocity and pressure field respectively,  $\rho$  is the fluid density,  $\mu$  is the dynamic viscosity,  $\mathbf{g}$  is the gravitational acceleration,  $\mathbf{f}_\sigma$  is the surface tension force defined as function of the temperature  $T$ , subscripts  $d$  and  $c$  are used for the dispersed and continuous fluids respectively,  $n_d$  is the number of separated interfaces in the dispersed fluid [7], superscript  $T$  is the transpose operator, whereas  $H_d$  is the Heaviside step function that is one in  $\Omega_d$  and zero elsewhere.

The conservation of energy in the form of the temperature equation, can be written as

$$\frac{\partial T}{\partial t} + \nabla \cdot (\mathbf{v} T) = \frac{1}{\rho c_p} \nabla \cdot (\lambda \nabla T) \quad \text{in } \Omega \quad (3)$$

with  $\lambda$  the thermal conductivity, and  $c_p$  the heat capacity, defined as

$$\lambda = \lambda_d H_d + \lambda_c (1 - H_d) \quad c_p = c_{p,d} H_d + c_{p,c} (1 - H_d) \quad (4)$$

The two major challenges of simulating interfaces between different fluids are to maintain a sharp front and to compute the surface tension accurately [9]. Regarding the first issue, the conservative level-set method (CLS) [8] deployed by [6] in the framework of unstructured meshes has been selected for interface capturing. Moreover, multiple level-set functions are used in order to avoid the coalescence of the fluid particles, according to the work reported by [7]. Therefore, the interface of the  $i$ -th fluid particle is defined as the 0.5 iso-surface of a regularized indicator function  $\phi_i$ , where  $i = 1, 2, \dots, n_d$  and  $n_d$  is the total number of fluid particles contained by the dispersed phase. The  $i$ -th interface transport equation can be written in conservative form provided the velocity field is solenoidal,  $\nabla \cdot \mathbf{v} = 0$ , namely,

$$\frac{\partial \phi_i}{\partial t} + \nabla \cdot \phi_i \mathbf{v} = 0, \quad i = 1, 2, \dots, n_d \quad (5)$$

Furthermore, an additional re-initialization equation is introduced in order to keep a sharp and constant interface profile

$$\frac{\partial \phi_i}{\partial \tau} + \nabla \cdot \phi_i (1 - \phi_i) \mathbf{n}_i = \nabla \cdot \varepsilon \nabla \phi_i, \quad i = 1, 2, \dots, n_d \quad (6)$$

This equation is advanced in pseudo-time  $\tau$  up to steady state. It consists of a compressive term,  $\phi_i (1 - \phi_i) \mathbf{n}_i|_{\tau=0}$ , which forces the level-set function to be compressed onto the interface along the normal vector  $\mathbf{n}_i$ , and of a diffusion term  $\nabla \cdot \varepsilon \nabla \phi_i$  that ensure the profile remains of characteristic thickness  $\varepsilon = 0.5h^{0.9}$ , with  $h$  defined as the grid size. The reader is referred to [6] for technical details on the selection of  $\varepsilon$ .

Geometrical information on the interface  $\Gamma_i$ , such as normal vector  $\mathbf{n}_i$  or curvature  $\kappa_i$ , is obtained through:

$$\mathbf{n}_i(\phi_i) = \frac{\nabla \phi_i}{\|\nabla \phi_i\|} \quad \kappa_i(\phi_i) = -\nabla \cdot \mathbf{n}_i, \quad i = 1, 2, \dots, n_d \quad (7)$$

Surface tension forces are calculated by the continuous surface force model [10], which is adapted to the multiple-marker/level-set method introduced by [7], and extended to take into account the variation of surface tension with temperature

$$\mathbf{f}_\sigma = \sum_{i=1}^{i=n_d} (\sigma(T)\kappa_i(\phi_i)\mathbf{n}_i - \nabla\sigma(T) + \mathbf{n}_i(\mathbf{n}_i \cdot \nabla)\sigma(T)) \|\nabla\phi_i\| \quad (8)$$

The surface tension coefficient is taken to be a linearly decreasing function of the temperature

$$\sigma = \sigma_0 - \sigma_T (T - T_0) \quad (9)$$

where  $\sigma_T = -d\sigma/dT = \text{constant}$ ,  $\sigma_0$  is the surface tension at the reference temperature  $T_0$ .

Furthermore, in order to avoid numerical instabilities at the interface, fluid properties in Eq. 2 and Eq. 4 are regularized by means of a global level-set function  $H_d = \phi_d$  [7]

$$\phi_d(\mathbf{x}, t) = \max\{\phi_1(\mathbf{x}, t), \dots, \phi_{n_d-1}(\mathbf{x}, t), \phi_{n_d}(\mathbf{x}, t)\} \quad (10)$$

Following the work introduced by [6], the Navier-Stokes equations, Eq. (1), and energy equation, Eq. (3), have been discretized by means of the finite-volume method on a collocated unstructured grid. A TVD-Superbee limiter scheme [11, 6] is used to approximate the convective term of momentum Eq. (1), energy Eq. (3) and interface transport Eq. (5); while diffusive terms are centrally differenced. A distance-weighted linear interpolation is used to find the cell face values of physical properties and interface normals, while gradients are computed at cell centroids by using the least-squares method [6]. Regarding the re-initialization Eq. (6), a central difference scheme is used to discretize both convective and diffusive terms.

Thus, the global algorithm can be summarized as follows

- (i) Initialize  $\mathbf{v}(\mathbf{x}_P, 0)$ ,  $\phi(\mathbf{x}_P, 0)$ , physical properties and interface geometric properties.
- (ii) The time increment,  $\Delta t$ , is calculated taken into account the CFL conditions and the stability condition for the capillary force [10]. Detailed information is given in [6].
- (iii) The interface is advected by means of the CLS method deployed in [6].
- (iv) Eq. 3 is solved for the temperature field using an explicit Euler discretization in time.
- (v) Physical properties ( $\rho, \mu, \lambda, c_p$ ) are updated at each control volume, whereas surface tension coefficient,  $\sigma(T)$ , is calculated by Eq. (9).
- (vi) The velocity field is computed by means of a fractional-step method [12] adapted to collocated unstructured grids with variable density, as is explained in [6].
- (vii) In order to avoid pressure-velocity decoupling when the pressure projection is made on collocated meshes [13], a cell face velocity  $\mathbf{v}_f$  is calculated so that  $\nabla \cdot \mathbf{v} = 0$  at each control volume [6]. Namely in discretized form:

$$\mathbf{v}_f = \sum_{q \in \{P, F\}} \frac{1}{2} \left( \mathbf{v}_q^{n+1} + \frac{\Delta t}{\rho(\phi_q^n)} (\nabla_h p^{n+1})_q \right) - \frac{\Delta t}{\rho_f} (\nabla_h p^{n+1})_f \quad (11)$$

where  $P$  and  $F$  are denoting the adjacent cell nodes with a common face  $f$ .

- (viii) Repeat steps ii-vii until time step required.

The reader is referred to [6, 7, 14, 15] for technical details on the finite-volume discretization and numerical methods used to solve the Navier-Stokes and Level-set equations on unstructured meshes. Further verification and validation of the CLS model used in this work, in the context of isothermal flows with constant surface tension can be found in [6, 7, 14]. The present numerical algorithms were implemented in the framework of a parallel C++/MPI code called TermoFluids [16].

Mesh	$(D_\Omega, H_\Omega)$	Cells	Cells/plane	$N_{planes}$	Cell geometry	$h$
$M1$	$(8d, 8d)$	$9.40 \times 10^5$	4700	200	hexahedral	$d/25$
$M2$	$(8d, 8d)$	$1.79 \times 10^6$	7440	240	hexahedral	$d/30$
$M3$	$(8d, 8d)$	$2.78 \times 10^6$	9940	280	hexahedral	$d/35$
$M4$	$(8d, 8d)$	$4.09 \times 10^6$	12800	320	hexahedral	$d/40$

**Table 1.** Mesh parameters used in 3D simulations of thermocapillary motion of isolated fluid particles. Here  $N_{planes}$  is the number of planes in which the symmetry axis of  $\Omega$  is divided.

### 3. Numerical results and discussion

The Marangoni motion of bubbles and drops can be characterized in terms of the following non-dimensional parameters

$$Ma = \frac{U_r(d/2)\rho_c c_{p,c}}{\lambda_c} \quad Re = \frac{U_r(d/2)\rho_c}{\mu_c} \quad Ca = \frac{U_r \mu_c}{\sigma_0} \quad (12)$$

$$\eta_\rho = \frac{\rho_d}{\rho_c} \quad \eta_\mu = \frac{\mu_d}{\mu_c} \quad \eta_\lambda = \frac{\lambda_d}{\lambda_c} \quad \eta_{c_p} = \frac{c_{p,d}}{c_{p,c}} \quad (13)$$

where the subindex  $c$  refers to the continuous phase, the subindex  $d$  refers to the drop fluid phase,  $U_r = \sigma_T ||\nabla T_\infty|| (d/2)/\mu_c$  is the named thermocapillary velocity,  $d$  is the initial droplet diameter,  $||\nabla T_\infty||$  is the temperature gradient imposed in the continuous fluid,  $Re$  is the Reynolds number,  $Ma$  is the Marangoni number,  $Ca$  is the capillary number, whereas  $\{\eta_\rho, \eta_\mu, \eta_\lambda, \eta_{c_p}\}$  are the ratios of physical properties. In addition,  $L_r = d/2$ ,  $U_r$  and  $T_r = (d/2)||\nabla T_\infty||$  denote the characteristic scales of length, velocity and temperature. Therefore the dimensionless velocity,  $V^* = (\mathbf{e}_y \cdot \mathbf{v}_c)/U_r$  with  $\mathbf{v}_c = \int_\Omega \phi \mathbf{v} dV / \int_\Omega \phi dV$ , and dimensionless time,  $t^* = 2tU_r/d$ , will be used to express the numerical results.

The present model is used to simulate the thermocapillary migration of a drop in an ambient liquid without gravity. The fluids are initially at rest and the temperature linearly increases from the cold bottom wall toward the hot top wall

$$T(x, y, z) = T_b + \frac{T_t - T_b}{H_\Omega} y = T_b + ||\nabla T_\infty|| y \quad (14)$$

with  $T_t$  the temperature of the top wall and  $T_b$  the temperature of the bottom wall.

In present simulations, a 3D cylindrical domain  $\Omega$  of diameter  $D_\Omega = 8d$  and height  $H_\Omega = 8d$  is considered.  $\Omega$  is divided by hexahedral control volumes generated by a constant step extrusion  $h = H_\Omega/N_{planes}$ , of a two-dimensional unstructured grid of quadrilateral cells along the symmetry axis of  $\Omega$ , as is summarized in Table 1. In order to maximize the droplet resolution, the mesh was concentrated around the symmetry axis of  $\Omega$  using a constant grid size,  $h$ , which grows exponentially to the border where it reaches a maximum size. A spherical drop of diameter  $d$  is placed on the symmetry axis of  $\Omega$ , at  $1.5d$  above the bottom wall. No-slip boundary conditions are applied on the top and bottom walls, and Neumann boundary condition is used on the lateral wall.

In the limit of zero Marangoni number and small Reynolds number, [3] derived the named YGB theory for the prediction of the steady state migration velocity ( $U_{YGB}$ ) of a drop in an infinite domain with constant temperature gradient field,  $||\nabla T_\infty||$ , such that the convective transport of momentum and energy are negligible

$$\frac{U_{YGB}}{U_r} = \frac{2}{(2 + 3\mu_d/\mu_c)(2 + \lambda_d/\lambda_c)} \quad (15)$$

where all the physical properties are assumed to be constant except for the surface tension, which is assumed to vary linearly with temperature.

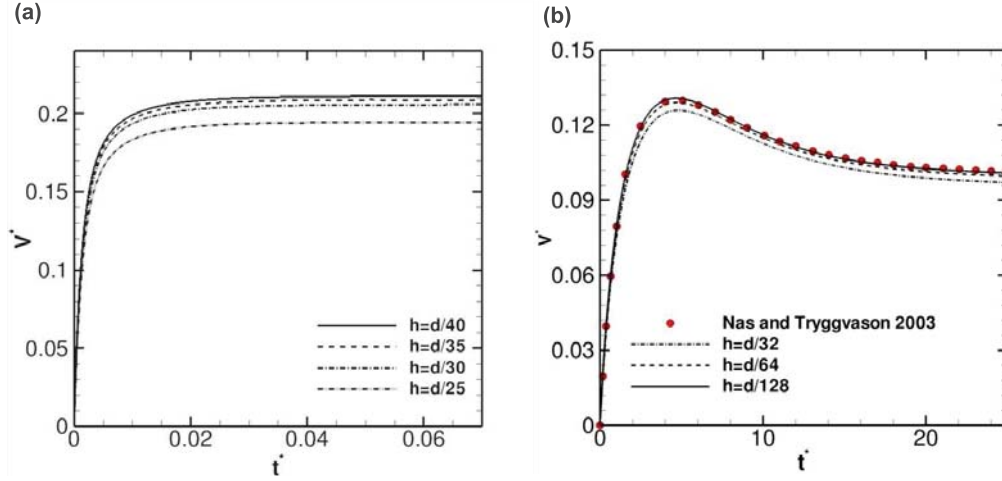


**Figure 1.** Migration velocity versus time. (a)  $Re = Ma = Ca = 0.066$ ,  $\eta_\rho = \eta_\mu = \eta_{c_p} = \eta_\lambda = 1.0$ . (b)  $Re = Ma = 0.01$ ,  $Ca = 0.0166$ ,  $\eta_\rho = \eta_\mu = \eta_{c_p} = \eta_\lambda = 0.5$ .

	Mesh			
	$M_1$	$M_2$	$M_3$	$M_4$
$V^*$	0.1946	0.2057	0.2088	0.2112
$\varepsilon_r$	7.9%	2.6%	1.1%	—

**Table 2.** Grid convergence of  $V^*$ , for  $Re = Ma = 0.01$ ,  $Ca = 0.0166$ ,  $\eta_\rho = \eta_\mu = \eta_{c_p} = \eta_\lambda = 0.5$ , and  $\varepsilon_r = |(V^* - V_{h=d/40}^*)/V_{h=d/40}^*|$ .

A first test case is simulated in the limit of low  $Ma$  and  $Re$  numbers, with  $Re = Ma = 0.01$ ,  $Ca = 0.0166$ ,  $\eta_\rho = \eta_\mu = \eta_{c_p} = \eta_\lambda = 0.5$ . For these parameters, the theoretical migration velocity of a spherical drop, calculated by means of Eq. 15, is  $U_{YGB}/U_r = 0.2285$ . Fig. 1a shows the temporal evolution of the dimensionless migration velocity,  $V^* = (\mathbf{e}_y \cdot \mathbf{v})/U_r$ , versus dimensionless time,  $t^*$ , using the present method with different grid resolutions. The influence of the grid size,  $h$ , is summarized in Table 2. It is found that the difference in the calculated migration velocities is no more than 1% between the meshes with  $h = d/35$  and  $h = d/40$ , therefore the finest mesh resolution  $h = d/40$  is selected for discussion of the results.

Fig. 1a also shows that the proposed numerical method converges to an asymptotic value  $V^*/U_{YGB} = 0.96$  which is comparable to the value 0.96 reported in [17] using a level-set model, and the value 0.97 calculated by [18] using the front-tracking method [9]. The slower rise velocities in the finite domain simulations compared with the theoretical migration velocity for the unbounded problem is probably due to the confinement effect. Thus, the proposed method to include variable surface tension in the framework of the finite-volume/level-set method [6] yields to stable results, consistent in accuracy with other state-of-art methods from the literature.

As further validation, the proposed numerical method is used to solve a 2D test case introduced by [19]. The material property ratios  $\eta_\rho$ ,  $\eta_\mu$ ,  $\eta_{c_p}$  and  $\eta_\lambda$  are set to 0.5, whereas the nondimensional parameters are chosen as  $Re = 5$ ,  $Ma = 20$ , and  $Ca = 0.01666$ . The computational domain is a rectangle extending  $4d$  in the  $x$  direction and  $8d$  in the  $y$  direction, where  $d$  is the drop diameter. The drop is initially located to the distance  $d$  above the bottom wall, on the vertical symmetry axis of the rectangular domain. The top and bottom walls are no-slip boundaries with constant temperature, and the horizontal boundaries are periodic.

Figure 1b presents the migration velocity of the drop versus time, computed by means of the

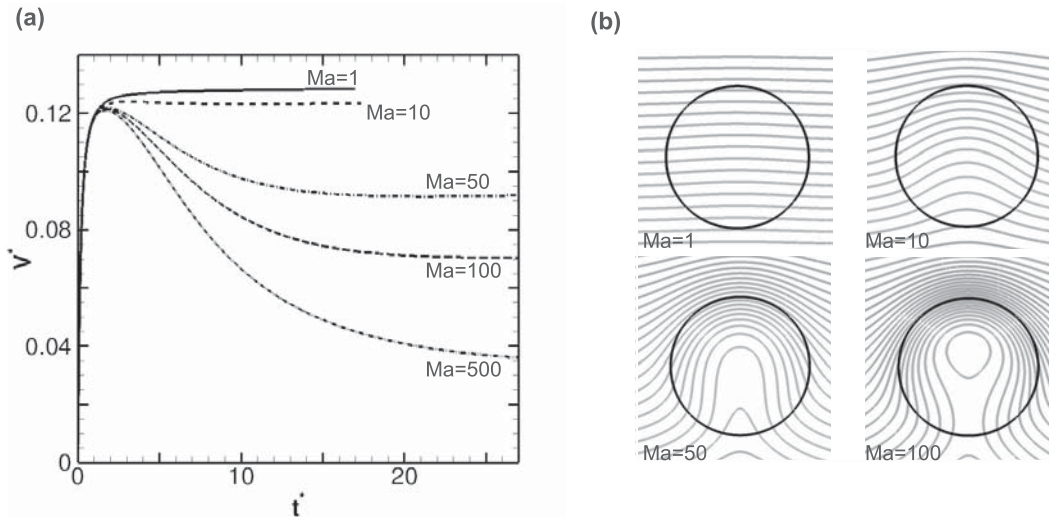


**Figure 2.**  $Re = 5$ ,  $Ma = \{1, 10, 50, 100\}$ ,  $Ca = 0.1$ ,  $\eta_\rho = \eta_\mu = \eta_{c_p} = \eta_\lambda = 1.0$  (a) Migration velocity versus time. (b) Isotherms at  $t^* = 40$ , with  $h = d/35$ , mesh  $M_3$  in Table 1.

present method, on uniform cartesian meshes with  $64 \times 128$ ,  $128 \times 256$  and  $256 \times 512$  grid points. It is clear from the aforementioned Figure that present computations are in excellent agreement with results reported by [19] using the front-tracking method [9]. Moreover, it is observed that  $V^*$  converges with mesh refinement, whereas the difference in  $V^*$  calculated with  $h = d/128$  and  $h = d/64$  is below 1.2%.

Fig. 2 shows the effect of the Marangoni number on the migration velocity of the droplet, for  $Re = 5$ ,  $Ma = \{1, 10, 50, 100\}$ ,  $Ca = 0.1$ ,  $\eta_\rho = \eta_\mu = \eta_{c_p} = \eta_\lambda = 1.0$ , computed on the mesh  $M_3$  as is described in Table 1. It is observed from Fig. 2a that an increase on  $Ma$  leads to a decrease in the migration velocity, which is consistent with simulation results reported by [20], [21] and [22]. Fig. 2b presents temperature contours at different Marangoni numbers, furthermore, it is observed that the convective transport of momentum and energy as  $Ma$  increases, results in a major distortion of the isotherms. Contrary to cases with  $Ma \sim 1$ , where the contours are almost a straight line, in cases with  $Ma \gg 1$  the isotherms tend to wrap around the drop.

Finally, the ability of the proposed level-set model is proved by simulating the Marangoni motion of 9 drops for  $Re = 40$ ,  $Ma = 40$ ,  $Ca = 0.0416\bar{6}$ ,  $\eta_\rho = \eta_\mu = \eta_{c_p} = \eta_\lambda = 0.5$ . The domain consists of a rectangular box with  $L_x \times L_y \times L_z = 4d \times 8d \times 4d$ , where  $d$  is the droplet diameter. It is discretized using a uniform cartesian mesh of  $160 \times 160 \times 320$  grid points, which is equivalent to  $8.192 \times 10^6$  control volumes or  $h = d/40$ . No-slip boundary condition is applied in all the walls, constant temperatures  $T_h$  and  $T_c$  are fixed on the top and bottom boundaries respectively, with  $T_h > T_c$ , whereas lateral walls are adiabatic. Nine equal size drops are placed arbitrary close to the lower cold wall. Fig. 3 shows the time evolution of migration velocities and vertical component of the drop centroids. Fig. 4 presents the visualization of the temperature contours on the plane  $z = 0$ , and the position of the drops at the time  $t^* = 65$ . From these figures, it is evident the formation of a layer of drops located on the same horizontal plane as the time increases. Moreover, droplets do not collide with the wall during the migration process. These results are consistent with qualitative descriptions reported by [19, 23] using the front tracking method [9].



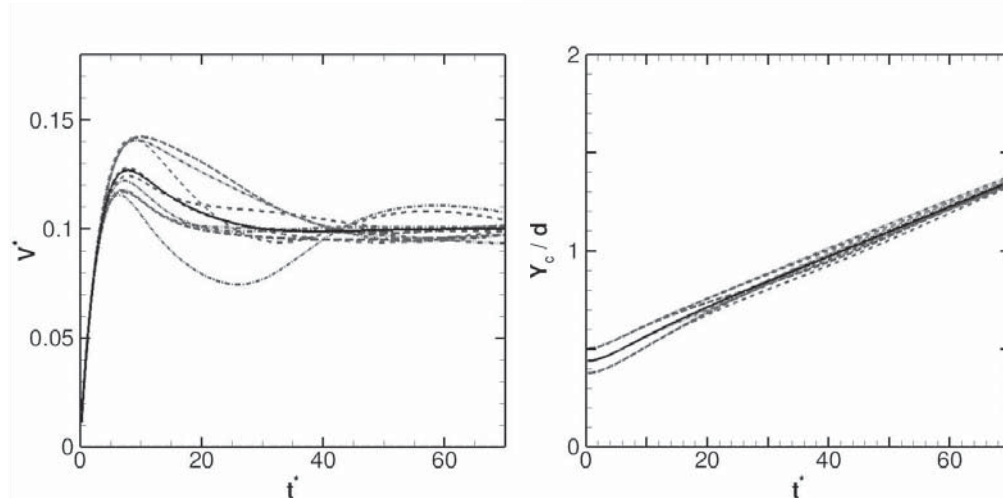


**Figure 3.** Thermocapillary interaction of 9 drops,  $Re = 40$ ,  $Ma = 40$ ,  $Ca = 0.046\bar{6}$ ,  $\eta_\rho = \eta_\mu = \eta_{c_p} = \eta_\lambda = 0.5$  (a) Migration velocity versus dimensionless time. (b) Droplet centroids versus dimensionless time.

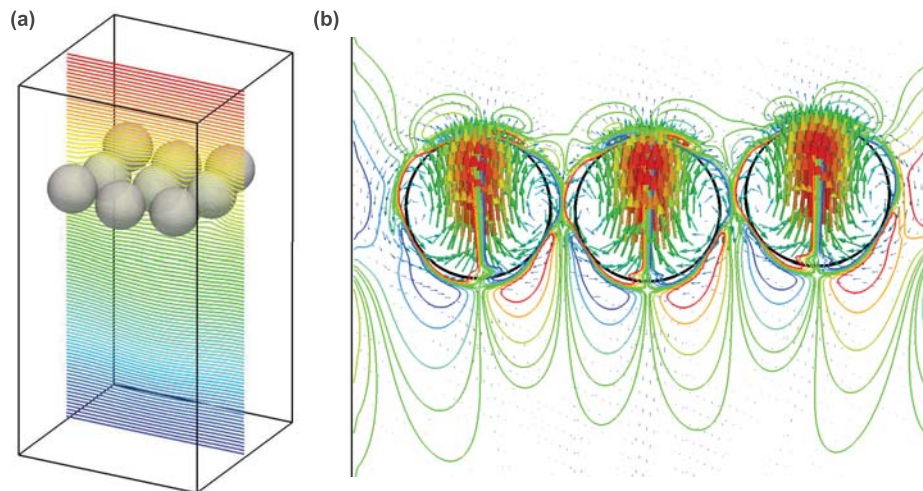


**Figure 4.** Thermocapillary interaction of 9 drops,  $Re = 40$ ,  $Ma = 40$ ,  $Ca = 0.046\bar{6}$ ,  $\eta_\rho = \eta_\mu = \eta_{c_p} = \eta_\lambda = 0.5$  (a) Temperature contours at  $z = 0$  at  $t^* = 65$ . (b) Vorticity contours and velocity vectors on the plane  $z = 0$  and time  $t^* = 65$ .

#### 4. Conclusions

In this paper, a level-set model for two-phase flows with thermocapillary effects at deformable interfaces has been introduced, which allows to the incompressible fluids to have different physical properties. To the best of the author's knowledge, this is the first time that thermocapillary effects are modeled in the framework of the conservative level-set method [6, 7]. The model has been validated against theoretical and numerical results from the literature, and then it has been used to explore the thermocapillary interaction of 9 droplets, avoiding the numerical coalescence of the fluid particles. Present results demonstrate that the proposed level-set model

is a reliable and accurate method for numerical simulation of thermocapillary flow. In future work, the present model could be extended to include surfactants and phase change phenomena.

## Acknowledgments

This work has been financially supported by the *Ministerio de Economía y Competitividad, Secretaría de Estado de Investigación, Desarrollo e Innovación*, Spain (ENE2011-28699), and by Termo Fluids S.L. Néstor Balcázar acknowledges financial support of the *Programa Torres Quevedo, Ministerio de Economía y Competitividad, Secretaría de Estado de Investigación, Desarrollo e Innovación* (PTQ-14-07186), Spain. Three-dimensional simulations were carried out using computer time provided by PRACE (project 2014112666) through the MareNostrum III supercomputer based in Barcelona, Spain.

## References

- [1] Subramanian, R.S., Balasubramaniam, R., The Motion of Bubbles and Drops in Reduced Gravity, Cambridge University Press, 2001.
- [2] Darhuber, A. A., Troian, S. M. 2005. Principles of microfluidic actuation by modulation of surface stresses. *Annu. Rev. Fluid Mech.* 37, 425-455.
- [3] Young, N. O., Goldstein, J. S., Block, M. J. 1959. The motion of bubbles in a vertical temperature gradient. *J. Fluid Mech.* 6, 350-356.
- [4] Subramanian, R.S., Slow migration of a gas bubble in a thermal gradient. *AIChE J.* 27, 646-654.
- [5] Subramanian, R.S., Thermocapillary migration of bubbles and droplets, *Adv. Space Res.* 3, 145-150.
- [6] Balcázar, N., Jofre, L., Lehmkuhl, O., Castro, J., Rigola, J., 2014. A finite-volume/level-set method for simulating two-phase flows on unstructured grids. *International Journal of Multiphase Flow* 64, 55-72
- [7] Balcázar, N., Lehmkuhl, O., Rigola, J., Oliva, A., 2015. A multiple marker level-set method for simulation of deformable fluid particles. *International Journal of Multiphase Flow* 74, 125-142
- [8] Olsson, E., Kreiss, G., 2005. A conservative level set method for two phase flow, *J. Comput. Phys.* 210, 225-246.
- [9] Tryggvason, G., Bunner, B., Esmaeeli, A., Juric, D., Al-Rawahi, N., Tauber, W., Han, J., Nas, S., Jan, Y.-J., 2001. A Front-Tracking Method for the Computations of Multiphase Flow, *J. Comput. Phys.* 169, 708-759.
- [10] Brackbill, J.U., Kothe, D.B., Zemach, C., 1992. A Continuum Method for Modeling Surface Tension, *J. Comput. Phys.* 100, 335-354.
- [11] Sweby, P.K., 1984. High Resolution Using Flux Limiters for Hyperbolic Conservation Laws, *SIAM Journal on Numerical Analysis* 21, 995-1011.
- [12] Chorin, A.J., Numerical solution of the Navier-Stokes equations. 1968. *Math. Comput.* 22, 745-762.
- [13] Rhie, C.M., Chow, W.L., 1983. Numerical Study of the Turbulent Flow past an Airfoil with Trailing Edge Separation, *AIAA J.* 21, 1525-1532.
- [14] Balcázar, N., Lemhkuhl, O., Jofre, L., Oliva, A., 2015. Level-set simulations of buoyancy-driven motion of single and multiple bubbles. *International Journal of Heat and Fluid Flow* 56, 91-107
- [15] Balcázar, N., Lehmkuhl, O., Jofre, L., Rigola, J., Oliva, A. 2016. A coupled volume-of-fluid/level-set method for simulation of two-phase flows on unstructured meshes. *Computers and Fluids* 124, 12-29
- [16] Lehmkuhl, O., Perez-Segarra, C.D., Soria, M., Oliva, A., 2007. A new Parallel unstructured CFD code for the simulation of turbulent industrial problems on low cost PC cluster, *Proceedings of the Parallel CFD 2007 Conference*, pp.1-8
- [17] Brady, P.T., Herrmann, M., Lopez, J.M., 2011. Confined thermocapillary motion of a three-dimensional deformable drop, *Physics of Fluids* 23, 022101
- [18] Muradoglu, M., Tryggvason, G., 2008. A front-tracking method for computation of interfacial flows with soluble surfactants, *J. Comput. Phys.* 227, 2238-2262.
- [19] Nas, S., Tryggvason, G., 2003. Thermalcapillary interaction of two bubbles or drops. *Int. J. Multiph. Flow* 29, 1117-1135.
- [20] Yin, Z., Gao, P., Hu, W., Chang, L. 2008. Thermocapillary migration of nondeformable drops, *Phys. Fluids* 20, 082101
- [21] Zhao, J.F., Li, Z.D., Li, H.X., Jing, L., 2010. Thermocapillary Migration of Deformable Bubbles at Moderate to Large Marangoni Number in Microgravity, *Microgravity Sci. Technol.* 22, 295-303
- [22] Guo, Z., Lin, P., 2015. A thermodynamically consistent phase-field model for two-phase flows with thermocapillary effects, *J. Fluid Mech.* 766, 226-271.
- [23] Nas, S., Muradoglu, M., Tryggvason, G., 2006. Pattern formation of drops in thermocapillary migration. *International Journal of Heat and Mass Transfer* 49, 2265-2276.